•研究论文•

DOI:10.15961/j.jsuese.201800337

Engineering Analysis of Strong Motion Data from Recent Earthquakes in Sichuan, China

HUANG Chen, *GALASSO Carmine*

(Department of Civil, Environmental and Geomatic Engineering, University College London (UCL), London WC1E 6BT, UK)

Abstract: Recent earthquakes in the Sichuan Province have contributed to significantly expand the existing ground-motion database for China with new, high-quality ground-motion records. This study investigated the compatibility of ground-motion prediction equations (GMPEs) established by the NGA-West2 project in the US and local GMPEs for China, with respect to magnitude scaling, distance scaling, and site scaling implied by recent Chinese strong-motion data. The NGA-West2 GMPEs for shallow crustal earthquakes in tectonically active regions are considerably more sophisticated than widely used previous models, particularly in China. Using a mixed-effects procedure, the study evaluated event terms (inter-event residuals) and intra-event residuals of Chinese data relative to the NGA-West2 GMPEs. Distance scaling was investigated by examining trends of intra-event residuals with source-to-site distance. Scaling with respect to site conditions was investigated by examining trends of intra-event residuals with soil type. The study also investigated other engineering characteristics of Chinese strong ground motions. In particular, the records were analyzed for evidence of pulse-like forward-directivity effects. The elastic median response spectra of the selected stations were compared to code-mandated design spectra for various mean return periods. Results showed that international and local GMPEs can be applied for seismic hazard analysis in Sichuan with minor modification of the regression coefficients related to the source-to-site distance and soil scaling. Specifically, the Chinese data attenuated faster than implied by the considered GMPEs and the differences were statistically significant in some cases. Near-source, pulse-like ground motions were identified at two recording stations for the 2008 Wenchuan earthquake, possibly implying rupture directivity. The median recorded spectra were consistent with the code-based spectra in terms of amplitude and shape. The new ground-motion data can be used to develop advanced ground-motion models for China and worldwide and, ultimately, for advancing probabilistic seismic hazard assessment (PSHA).

Key words: ground motion prediction equations; NGA-West2 project; code-based spectrum; pulse-like ground motions

中图分类号: P315.9　　文献标志码: A　　文章编号: 2096-3246(2018)03-0112-13

Sichuan Province is one of the most earthquake-prone areas in China. Recently, the 2008 M_S 8.0 (M_W 7.9) Wenchuan earthquake, the 2013 M_S 7.0 (M_W 6.6) Lushan earthquake, and the 2017 M_S 7.0 (M_W 6.5) Jiuzhaigou earthquake have stricken Sichuan, causing vast socio-economic loss. These three events were well-recorded by the National Strong Motion Observation Network System (NSMONS) of China, which has been in full operation since 2008. These records represent abundant new data for earthquake engineering and engineering seismology research in China, particularly for the development of new ground-motion models for probabilistic seismic hazard analysis (PSHA). PSHA represents the first step of probabilistic seismic risk assessment and performance-based earthquake engineering (PBEE). The assessment of seismic risk represents, in turn, the first step towards the development of risk reduction strategies.

Ground motion prediction equations (GMPEs), also known as ground-motion models and attenuation relations, are a key component in PSHA. They are empirical models estimating the probability distribution of ground-motion intensity measures (*IM*s; e.g., peak ground accel-

收稿日期:2018 – 03 – 27

基金项目:Community Based Disaster Management in Asia Programme Phase Ⅱ (CBDM Asia Phase Ⅱ) (00084327)

作者简介:HUANG Chen (1992—), Female, PhD. Research direction: earthquake engineering. E-mail: chen.huang.14@ucl.ac.uk

网络出版时间:2018 – 05 – 06 00 : 06 : 00　　网络出版地址: http://kns.cnki.net/kcms/detail/51.1773.TB.20180506.0006.003.html

eration, *PGA*; spectral accelerations, S_a), occurring at a given site, as a function of magnitude, source-to-site distance, soil properties, focal mechanism, and other parameters. There are some limitations in the current GMPEs for China. For instance, the Huo89 model[1], a widely used and validated set of GMPEs for *PGA* and S_a for China, was developed using a conversion method proposed for regions with little ground-motion data[2], and considered only magnitude, source-to-site distance (in terms of epicentral distance, R_{epi}) and soil-type as predictors. Yu et al.[3] proposed a set of GMPEs for the latest, fifth-generation Chinese seismic zonation map using the same conversion method and including events up to 2008. However, the model of Yu et al. is only applicable to rock sites. None of the existing GMPE sets for China account for the style-of-faulting. Moreover, more complex effects, such as hanging-wall effect, ground-motion directivity, and nonlinear site response, have not been included in past Chinese GMPEs. This is because the required data/information is often difficult to obtain or must be estimated through empirical relations characterized by relatively high-uncertainty.

The NGA-West2 project, coordinated by the Pacific Earthquake Engineering Research Center (PEER), developed five advanced GMPEs[4–8] based on a global dataset of shallow crustal earthquakes in tectonically active regions, addressing the aforementioned issues.

Given the recent availability of high-quality recorded data in Sichuan, the applicability of the NGA-West2 models for this region is of special interest. The comparison between the extended ground-motion database for the Sichuan Province and the latest NGA-West2 models represent an important first step towards the future development of improved, more sophisticated GMPEs for Sichuan and, ultimately, for China.

To this aim, this study investigates the compatibility of international GMPEs established by the NGA-West2 project and the local Huo89 GMPEs to the ground-motion records from three major, recent events in the Sichuan Province. The model compatibility is investigated in terms of magnitude scaling, source-to-site distance scaling, and site scaling. A similar study was carried out for Italian data by Scasserra et al.[9] using the first generation NGA-West models[10–14], and showing, for instance, the Italian data attenuated faster than implied by the NGA models at short periods. Wang et al.[15] also compared the Wenchuan earthquake data with the NGA-West models and found that the Wenchuan earthquake was characterized by an inconsistent site scaling with respect to the site scaling from the NGA models. This paper also attempts to preliminarily investigate near-fault directivity effects in China by identifying pulse-like ground motions in the considered Chinese dataset. Finally, a comparison between the code-based spectra in China and recorded spectra for each event is presented. The considered code-based spectra are derived by the current Chinese Seismic Design Code for Buildings (GB50011—2010[16]) and the recently released seismic hazard map[17], which are also based on the lessons learned from the Wenchuan earthquake.

1 The strong-motion dataset

The dataset considered in this study has been provided by the China Earthquake Data Center at the China Earthquake Administration (CEA). The metadata for each considered event is listed in Tab. 1.

Tab. 1　Metadata for the three considered events in Sichuan

Event	Date	Epicentre latitude/(°)	Epicentre longitude/(°)	Depth/km	Fault style	M_W	M_S	Strike/(°)	Dip/(°)	Rake/(°)	Length/km	Width/km	Comp. number
Wenchuan*	2008-05-12	31.0	103.4	14	*FR*	7.9	8	229.4	32.0	118.3	308	40	404 (93)
Lushan+	2013-04-20	30.3	103.0	13	*FR*	6.6	7	205.0	38.5	88.8	66	35	123 (59)
Jiuzhaigou×	2017-08-08	33.2	103.8	20	*FS*	6.5	7	148.5	68.9	–3.1	57	27	67 (34)

Note: *FR* is the reverse fault; *FS* is the strike-slip fault; Comp. number is the total number of 3-component records, while the number of selected 3-component records with $R_{JB} \leq 250$ km is shown in brackets; the finite-fault models are obtained from * Wang et al.[18], + Wang et al.[19], × Wang et al.[20].

The scatter plot of moment magnitude M_W against the Joyner-Boore distance R_{JB} in km (i.e., the closest distance to the surface projection of the rupture plane) is presented in Fig. 1, where the data recorded at rock sites are represented through red circles and the records at soil sites are represented through green circles.

Several predictive variables are needed for the implementation of the NGA-West2 models and the China-specific models. The moment magnitude M_W is used in all the considered model. The finite-fault models are ob-

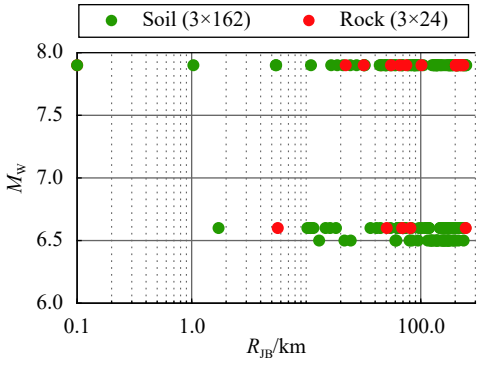

Fig. 1 Scatter plot of M_W against R_{JB} and total numbers of selected three-component (3 ×) records

tained from published studies[18–20], providing the strike, dip and rake angle, the width and length of rupture fault, and the depth to the top of the rupture (Z_{TOR}) in km (measured from the ground surface). Since the fault plane geometry is known, different distance metrics at the stations, required by the different ground-motion models, can be easily calculated, namely, the Joyner-Boore distance (R_{JB}/km), the closest distance to the rupture plane (R_{RUP}/km), the distance measured perpendicular to the fault strike from the surface projection of the up-dip edge of the fault plane (R_X/km). Moreover, the hanging-wall indicators are computed based on the finite-fault model according to the NGA-West2 definition. The region-specific parameters, e.g., *region* predictor[4–5], the coefficient of regional differences Δc_{20}[6], and the multiplicative adjustment factor γ[7] accounting for anelastic attenuation, are chosen for China accordingly.

The soil classification used for the NSMONS stations has only two categories, rock and soil, due to the lack of borehole data or any other type of detailed measurements. This two-category classification is different from the four-category site classification specified in the Chinese Code for Seismic Design of Buildings (GB 50011—2010). In fact, based on the cover layer thickness in m and V_{S20} in m/s, i.e., the average shear-wave velocity in the upper 20 m of the soil, the Chinese Code for Seismic Design of Buildings classifies a site into five possible classes, as described in Tab. 2.

This is similar to the six-category (A to F) site classification in the National Earthquake Hazards Reduction Program (NEHRP)[21] based on V_{S30}, the average shear-wave velocity in the upper 30 m soil in m/s. The cover layer thickness in m is the thickness of the soil layer above the rock, with shear-wave velocity > 500 m/s[16].

Tab. 2 Cover layer thicknessand V_{S20} for different site classes in the Chinese Code for Seismic Design of Buildings (GB50011—2010[16])

V_{S20}/(m·s^{-1})	Cover layer thickness/m				
	Site class				
	I_0	I_1	II	III	IV
V_{S20} >800	0				
800 ≥ V_{S20} >500		0			
500 ≥ V_{S20} >250		<5	≥ 5		
250 ≥ V_{S20} >150		<3	3～50	>50	
V_{S20} ≤ 150		<3	3～15	15～80	>80

The NGA-West2 models all require the knowledge of the V_{S30} parameter. Yu[22] obtained the borehole data and the resulting V_{S20} soil profiles for 147 stations in the Sichuan Province and the Gansu Province. Assuming the soil medium would be unchanged from the bottom of the borehole till a 30 m depth, Yu assumed $V_{S30} = V_{S20}$ for all stations; 80 stations out of the 147 above are used in this study (V_{S30} values at those 80 stations are denoted by $V_{S30,measured}$). Alternatively, the USGS V_{S30} Models and Data platform[23] provides an estimated V_{S30} value (denoted here as $V_{S30,estimated}$) for locations within latitude −56° to 84° and longitude −180° to 180° at 30 arc-seconds grid resolution, based on the global topographic slope. The $V_{S30,estimated}$ ranges from 98 m/s to 2 197 m/s and $V_{S30,estimated}$ = 600 m/s for water-covered areas. The scatter plot of $V_{S30,measured}$ against $V_{S30,estimated}$ for the 80 stations introduced above is shown in Fig. 2, highlighting that the $V_{S30,estimated}$ is, on average, higher than the $V_{S30,measured}$, especially in the range $V_{S30,measured}$ ≤ 500 m/s (red area).

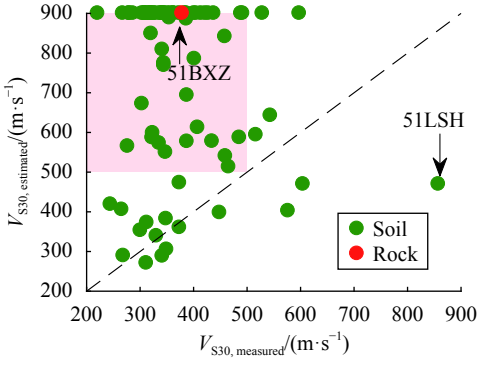

Fig. 2 Scatter plot of $V_{S30,measured}$ and $V_{S30,estimated}$ for the considered stations, colored by the two-category soil classification

According to the Chinese Code for Seismic Design of Buildings, V_{S20} > 500 m/s corresponds to the bedrock,

where the drilling of borehole test is stopped. Yu also stated that when the drilling depth was significantly less than 20 m, there may exist inaccuracy in the $V_{S30,measured}$ value. For example, station 51BXZ (red dot in Fig. 2) is located at a site classified as rock by NSMONS. According to the borehole data at this station, the depth of the borehole is 18.20 m and the medium at the bottom of the borehole has shear-wave velocity 658 m/s (considered as rock). Yu computed the average shear-wave velocity $V_{S30,measured}$ = 379 m/s (as hard soil, Class Ⅱ according to GB50011—2010) while the USGS gives $V_{S30,estimated}$ = 900 m/s as rock Class Ⅰ. Similarly, station 51LSH (the last green dot on the right) situates on a site classified as soil by NSMONS. The borehole depth of this station is 9.8 m when reaching the bedrock with shear-wave velocity 1 160 m/s. Yu computed $V_{S30,measured}$ = 858 m/s (as rock, Class Ⅰ) while USGS provides $V_{S30,estimated}$ = 470 m/s as hard soil, Class Ⅱ. Fig. 2 and these specific cases highlight the large uncertainty in the site classification and, in particular, in the simplified estimation of the V_{S30} values, which suggest there might be misclassifications of the site class at some locations. The V_{S30} parameter accounts for the local site conditions and its accuracy has a huge impact on the ground-motion models and its application. In fact, the local site conditions can modify the ground motion in terms of amplitude, frequency and duration. As shown above, available information at seismic stations are frequently inadequate for a proper site characterization and can have a significant impact on the definition of seismic hazard both at large and local scale. There is an urgent need to invest in site characterization of the recording stations in order to improve the current knowledge on strong motion seismology.

For the purpose of this study, the $V_{S30,measured}$ value at each station is used as the preferred value in the analysis and, if this data is not available, the $V_{S30,estimated}$ is used, instead.

2 Comparison with NGA-West2 GMPEs

2.1 Comparisons of the median prediction

The historical data are first visually compared with the estimates of *PGA*, and S_a at two representative periods, i.e., 0.1 and 1.0 s, from the NGA-West2 models and the Huo89 model, as shown in Fig. 3, where the plots in column refer to (a), (d), (g) Wenchuan earthquake; (b), (e), (h) Lushan earthquake; (c), (f), (i) Jiuzhaigou earthquakes, given V_{S30} = 360 m/s. For simplicity, the following acronyms are used hereinafter: ASK14 for the model of Abrahamson et al.[4]; BSSA14 for the model of Boore et al.[5]; CB14 for the model of Campbell and Bozorgnia[6]; CY14 for the model of Chiou and Youngs[7]; and I14 for the model of Idriss[8].

For illustrative purpose, the predictors are set as follows: V_{S30} = 360 m/s, similar to stiff soil D in NEHRP; R_{RUP} and R_{epi} are assumed to be equal to R_{JB}; fault geometry varies depending on events; no hanging-wall effect is assumed; region-specific parameters are chosen for China; other parameters (e.g., R_X; R_Y, the horizontal distance (km) from the top edge of the rupture, measured along fault strike; $Z_{1.0}$ depth in km to V_{S30} = 1.0 km/s; $Z_{2.5}$ depth in km to V_{S30} = 2.5 km/s; Z_{BOT} depth in km to the bottom of the seismogenic crust) are set as unknown.

It is worth noting that the geometric mean of the two horizontal ground-motion components is used in this study, while the NGA-West2 models use *RotD*50 (i.e., the median single-component horizontal ground-motion across all non-redundant azimuths). However, studies (e.g., Barani et al.[24]) show that the differences between the geometric mean and *RotD*50 are minimal (negligible at low periods and, generally, less than 5% ~ 8%). The impact of different *IM* definitions is under investigation by the authors.

As shown in Fig. 3 (a), (d), (g), there is an overall good compatibility for the Wenchuan earthquake between the NGA-West2 models and the historical data, for all the considered periods (i.e., 0, 0.1 and 1.0 s). This result is somehow expected as this event is included in the NGA-West2 database and in the calibration of the considered GMPEs. The Huo89 gives a similar median prediction to the NGA-West2 models but slight overestimates the spectral accelerations at 1.0 s. With respect to the Lushan earthquake in Fig. 3(b), (e), (h), the NGA-West2 models show a good compatibility with the observed *PGA* data, though they slightly underestimate the spectral accelerations at 0.1 s and overestimate them at 1.0 s. Huo89 model underestimates the observed *PGA* and $S_a(T = 0.1\ s)$ data for the Lushan earthquake but overestimates the $S_a(T = 1.0\ s)$ data. Finally, with respect to the Jiuzhaigou earthquake in Fig. 3(c),

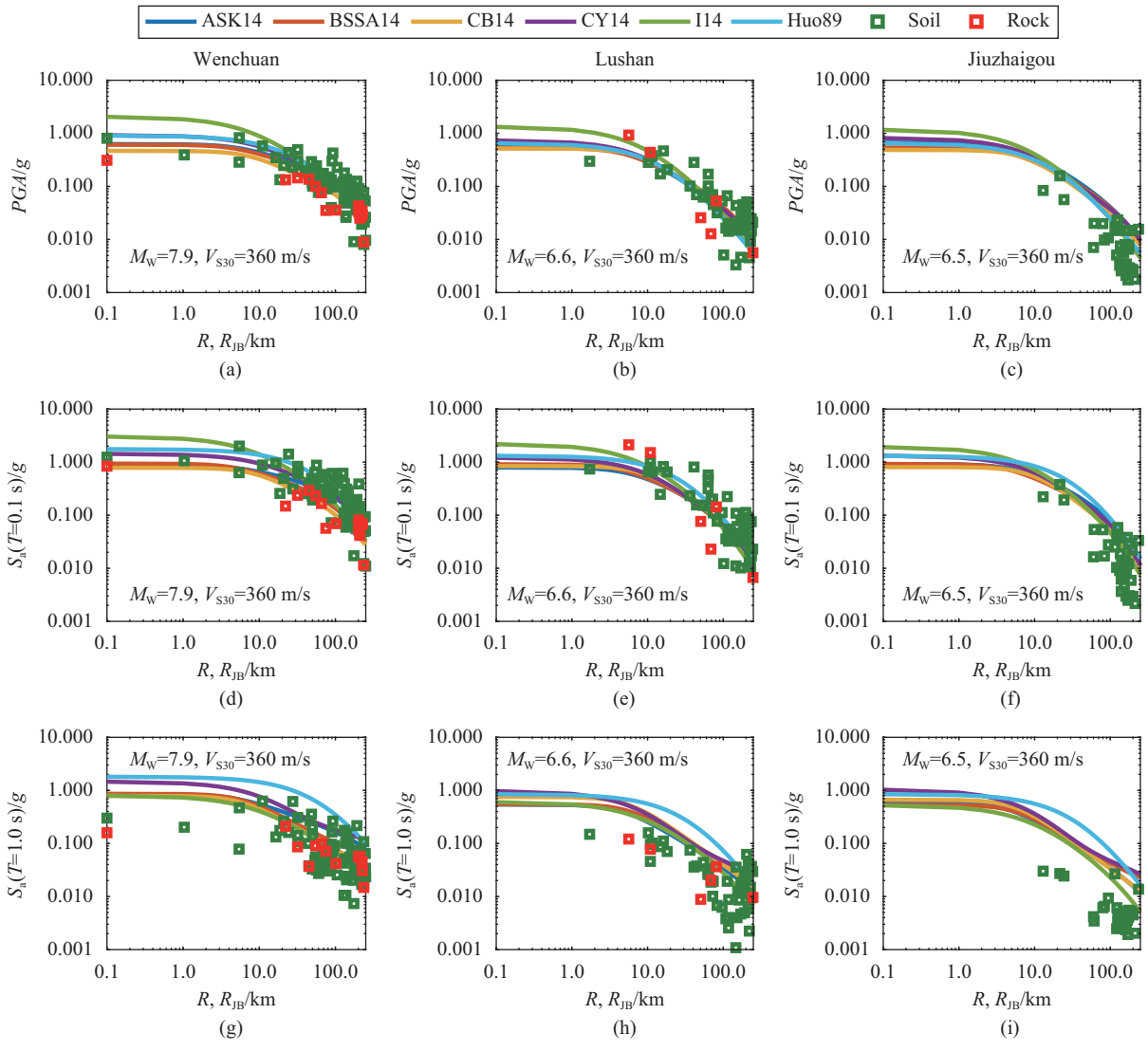

Fig. 3 Comparisons between the historical data and median predictions of (a)～(c) *PGA*, (d)～(f) $S_a(T = 0.1\ \text{s})$, (g)～(i) $S_a(T = 1.0\ \text{s})$

(f), (i), the NGA-West2 and Huo89 models significantly overestimate the observed *PGA* values and the considered spectral ordinates. Moreover, the Huo89 model gives a higher decay rate than the NGA-West2 models, particularly in the far-field.

The visual comparison of Fig. 3 shows that the NGA-West2 and Huo89 models may require some modification to be fully applicable to the Sichuan region. Either overestimation or underestimation of the actual data may result in biased seismic hazard and risk estimate, and consequently, in biased estimates of potential earthquake-induced loss (e.g., for insurance purposes, risk management, etc.).

2.2 GMPE bias and standard deviation

The previous section has introduced qualitative, visual-inspection based comparisons between the median predictions from the benchmark GMPEs and the Chinese data. This section provides a quantitative analysis of the compatibility of the NGA-West2 models and the Huo89 model with the Sichuan data. The residuals between the observed data and the median predictions from each considered GMPEs are evaluated at eight periods of 0 s (i.e., *PGA*), 0.1, 0.2, 0.3, 0.5, 1.0, 1.5, and 2.0 s, individually. The residuals are computed as in Eq. (1):

$$(r_{ij})_k = \ln IM_{ij,\text{obs}} - \ln(IM_{ij})_k \quad (1)$$

In Eq. (1), $(r_{ij})_k$ is the residual at site j for the event i given model k, $IM_{ij,\text{obs}}$ is the observed IM at site j for the event i, $(IM_{ij})_k$ is the median IM at site j for the event i calculated using the model k (in natural log units). For simplicity, subscript k will be omitted in the rest of the paper.

The analysis of residuals with respect to magnitude, source-to-site distance and site scaling requires the knowledge of the inter- and intra-event residuals. A linear mixed-effect regression is performed to calculate these quantities by the fitlme function in MATLAB, as in Eq. (2):

$$r_{ij} = c + \eta_i + \varepsilon_{ij} \quad (2)$$

In Eq. (2): c is the constant representing a mean offset (or bias) of the data relative to the selected GMPE k; η_i is the inter-event residual of event i with zero mean and τ standard deviation, accounting for the variability between events at the same site; ε_{ij} is the intra-event residual at site j of event i with zero mean, and σ standard deviation, accounting for the variability between different sites within the same event.

As shown in Fig. 4(a), the constant coefficient c and its 95 % confidence interval (denoting by the upper and lower bars) indicate that there would be a slight misfit between the Sichuan data and the NGA-West2 models and a huge discrepancy with respect to the Huo89 model, particularly at long periods. The trend of the constant coefficient c against periods is consistent among the six GMPEs. Regarding the NGA-West2 models, parameter c is slightly greater than zeros at short periods (T < 0.5 s) and lower than zeros at longer periods. This suggests that the NGA-West2 models would underestimate the observations at shorter periods and overestimate them at longer periods. The constant coefficient c does not significantly deviate from zero, when zero is not included within the confidence intervals (e.g., ASK14 and CY14 at period 0.2 s). The Huo89 model gives a coefficient c comparable with the NGA-West2 models but with higher variability, which results in the non-rejection of the statistical hypothesis c= 0. In fact, the Huo89 model is characterized by higher epistemic uncertainty due to the lack of information on various earthquake effects/regression variables.

The inter-event standard deviation τ and the intra-event standard deviation σ versus periods and their 95% confidence interval are also presented in Fig. 4(b) ~ (c). In terms of inter-event standard deviation τ, the NGA-West2 models generally give small values close to zero while Huo89 model provides a consistent standard deviation that is higher than the NGA-West2 models, which is possibly because the Huo89 model does not consider the style-of-faulting and other predictors and, thus, has a higher variability across events. The values obtained from the five NGA-West2 GMPEs are smaller than expected, which is possibly due to the amount of recordings for each event and the fact that two out of three events were caused by the same focal mechanism/fault. The intra-event standard deviations σ values computed from the NGA-West2 models are consistent, with little variations, while Huo89 produces higher estimates of σ with larger variabilities. The trend of σ against periods is consistent for all GMPEs.

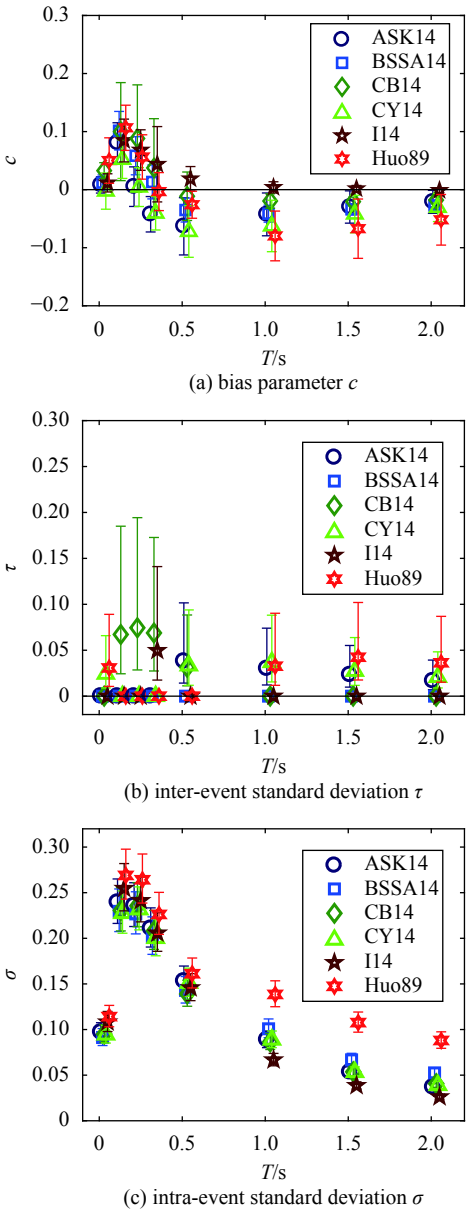

Fig. 4　Scatter plot of bias parameter c, inter-event standard deviation τ, and intra-event standard deviation σ for the six GMPEs against periods

The inter-event residual vector $\boldsymbol{\eta} = (\eta_i)$ is important to investigate the magnitude scaling. Due to the issues

discussed above, the inter-event residual $\boldsymbol{\eta}$ is relatively small and the magnitude scaling cannot be properly captured by analyzing $\boldsymbol{\eta}$. In addition, this study only considers three events and two of them have a very similar magnitude. However, the visual comparisons of Fig. 3 seem to suggest that the magnitude scaling is well-modeled for the three considered events. Thus, this study will further focus on the compatibility of the considered models with respect to source-to-site distance scaling and V_{S30}-based site effect implied by the China data.

2.3 Distance scaling

This section assesses the chosen models in characterizing the source-to-site distance scaling of the Sichuan data. It is assumed that the intra-event residuals are proportional to the logarithm of the source-to-site distance R. A linear regression is performed as in Eq. (3):

$$\varepsilon_{ij} = a_{\mathrm{R}} + b_{\mathrm{R}} \ln(R_{ij}) + \tilde{\varepsilon}_{ij} \quad (3)$$

In Eq. (3), a_{R} and b_{R} are the regression coefficients for the distance scaling, R_{ij} is the source-to-site distance in km at station j of event i, $\tilde{\varepsilon}_{ij}$ is the remaining intra-event residual at station j of event i that results from the fit of Eq. (3). The source-to-site distance uses R_{RUP} for models of ASK14, CB14, CY14 and I14, R_{JB} for the BSSA14 model, and R_{epi} for Huo89 model. The slope parameter b_{R} represents approximately the misfit of the distance scaling in the Sichuan dataset relative to the chosen GMPEs. The statistical t-test is used to study the significance level p of the distance dependence in the intra-event residuals. The null hypothesis H_0 to be tested is H_0: $b_{\mathrm{R}} = 0$, i.e., no distance dependence. For example, if $p < 0.05$ (or $1 - p > 0.95$), it is suggested there is significant statistical evidence to reject the null hypothesis H_0 and there is distance dependency in the data.

The results of the analysis are plotted in Fig. 5, where the red line is the median prediction and the black dashed lines represent the 95% confidence interval of the predictions. Fig. 5 shows that there is some distance dependency in the residuals of the considered models (each row corresponds to a ground-motion model). In particular, the CB14 model has a p-value less than 0.05 (i.e., $1-p > 0.95$) across the periods, indicating significant evidence to reject the zero slope null hypothesis. The distance dependency is also observed in ASK14 and Huo89 at short periods (PGA and $S_{\mathrm{a}}(T = 0.1\ \mathrm{s})$), for which the p-value is less than 0.05. The BSSA14, CY14 and I14 models present distance dependency in $S_{\mathrm{a}}(T = 0.1\ \mathrm{s})$ but unbiased distance attenuation in PGA and at long periods ($T \geq 1.0$ s). The negative slope values in the models and the statistically significant distance dependency suggest a faster decay in distance of the Sichuan data comparing to these GMPEs. Nonetheless, the absolute values of the slope are small in general, possibly due to the limited quantity of data.

According to the results in this section, the distance scaling in the NGA-West2 and Huo89 models needs to be adjusted to better capture the observed distance dependency in the Sichuan data. Thus, in the next sections, the intra-event residuals ε_{ij} are re-computed by removing the distance dependency defined by Eq. (3) and the remaining residuals, denoted by $\tilde{\varepsilon}_{ij}$, are studied regarding the V_{S30} shear-wave velocity.

2.4 Site effects

The scaling of ground motions with respect to the V_{S30} parameter is analyzed in this section. The remaining intra-event residuals $\tilde{\varepsilon}_{ij}$ are assumed to be proportional to the logarithm of the average shear-wave velocity V_{S30}. The linear model is structured as in Eq. (4):

$$\tilde{\varepsilon}_{ij} = a_{\mathrm{V}} + b_{\mathrm{V}} \ln(V_{S30,ij}) + \xi_{ij} \quad (4)$$

In Eq. (4), $\tilde{\varepsilon}_{ij}$ is the intra-event residual excluding the distance dependency at site j of event i in Eq. (3), a_{V} and b_{V} are the regression coefficients for site effect, ξ_{ij} is the error term.

The slope parameter b_{V} represents approximately the misfit of the V_{S30} scaling in the Sichuan dataset relative to the chosen GMPEs. The fitted results of the updated intra-event residuals $\tilde{\varepsilon}_{ij}$ against shear-wave velocity V_{S30} are shown in Fig. 6, where the red line is the median prediction and the black dashed lines are the 95% confidence interval of predictions (each row corresponds to a ground-motion model). The results show there is no evidence to reject the null hypotheses that $b_{\mathrm{V}} = 0$ at 5% significance, which is equivalent to not reject the assumption of no V_{S30} dependency, except for I14 across periods and CY14 for PGA. In general, the results suggest the V_{S30}-based site effect in the NGA-West2 models may be compatible with the Sichuan data, except for I14.

Compared to the NGA-West2 model, the Huo89 model used the discrete two-category site classification other than the continuous shear-wave velocity. However, a similar finding is observed between the Huo89 model

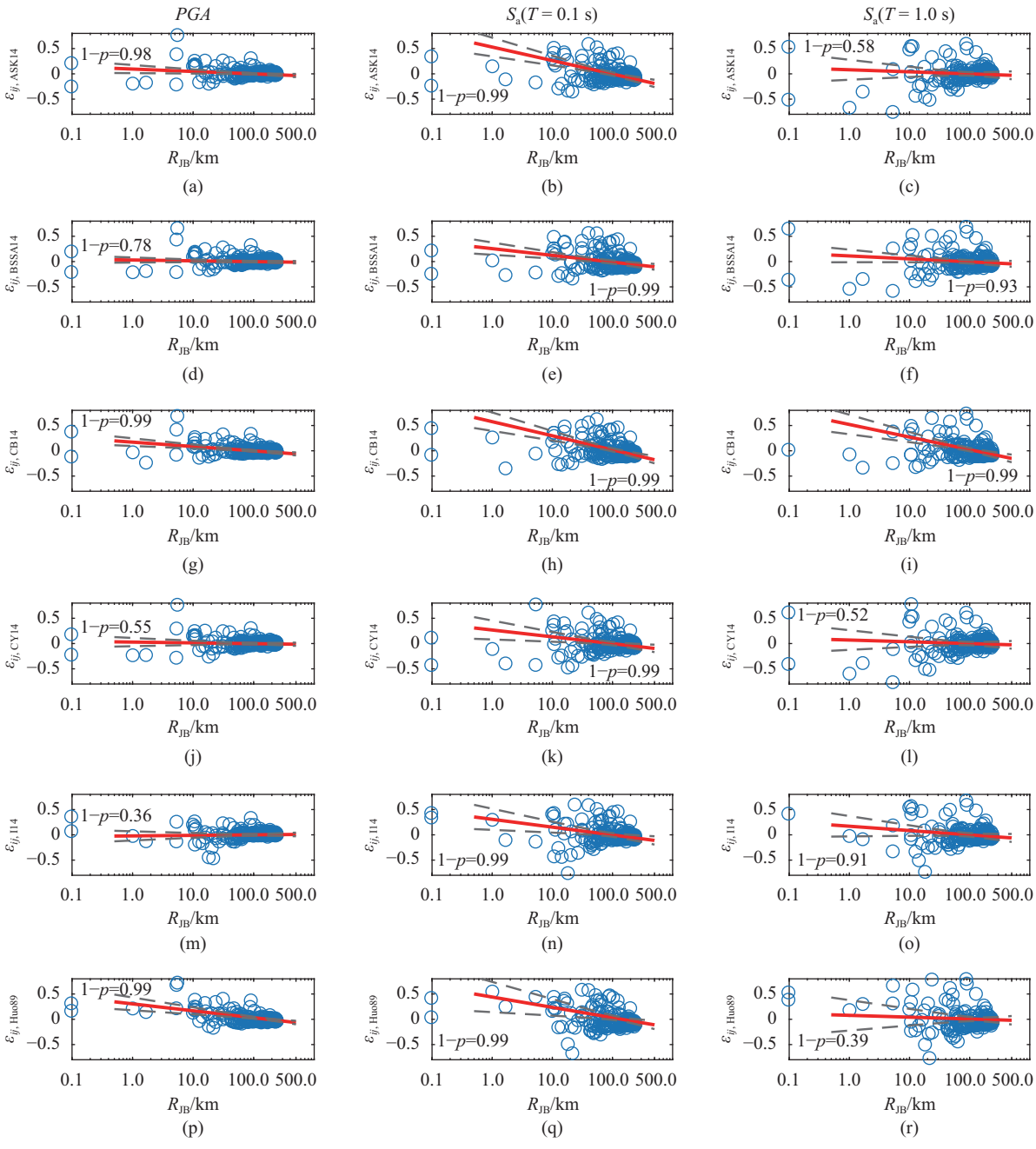

Fig. 5　Variation of intra-event residuals against R_{JB} for *PGA*, $S_a(T = 0.1$ s), $S_a(T = 1.0$ s)

and the NGA-West2 models. It may suggest the simplified site category may be a good proxy to partially account for site effect. The V_{S30} dependency is more notable in *PGA* than in spectral acceleration, which may be due to the deep geologic structure (i.e., basin effect) and nonlinear site effect.

2.5　Pulse-like near-source ground motions

A distinct, long-period velocity pulse often characterizes near-fault earthquake ground motions. Such pulse is typically observed at the beginning of the fault-normal ground velocity time-history and has a probability of occurrence that depends on the site-to-source geometry, earthquake magnitude and other parameters. The destructive potential of near-fault, pulse-like ground motions was evident after many earthquakes such as the Northridge earthquake, California (1994); Kobe earthquake, Japan (1995); Chi-Chi earthquake, Taiwan (1999); and L'Aquila earthquake, Italy (2009).

In this study, the presence of pulse-like ground motions in the considered Chinese dataset and the identification of pulse characteristics is achieved according to

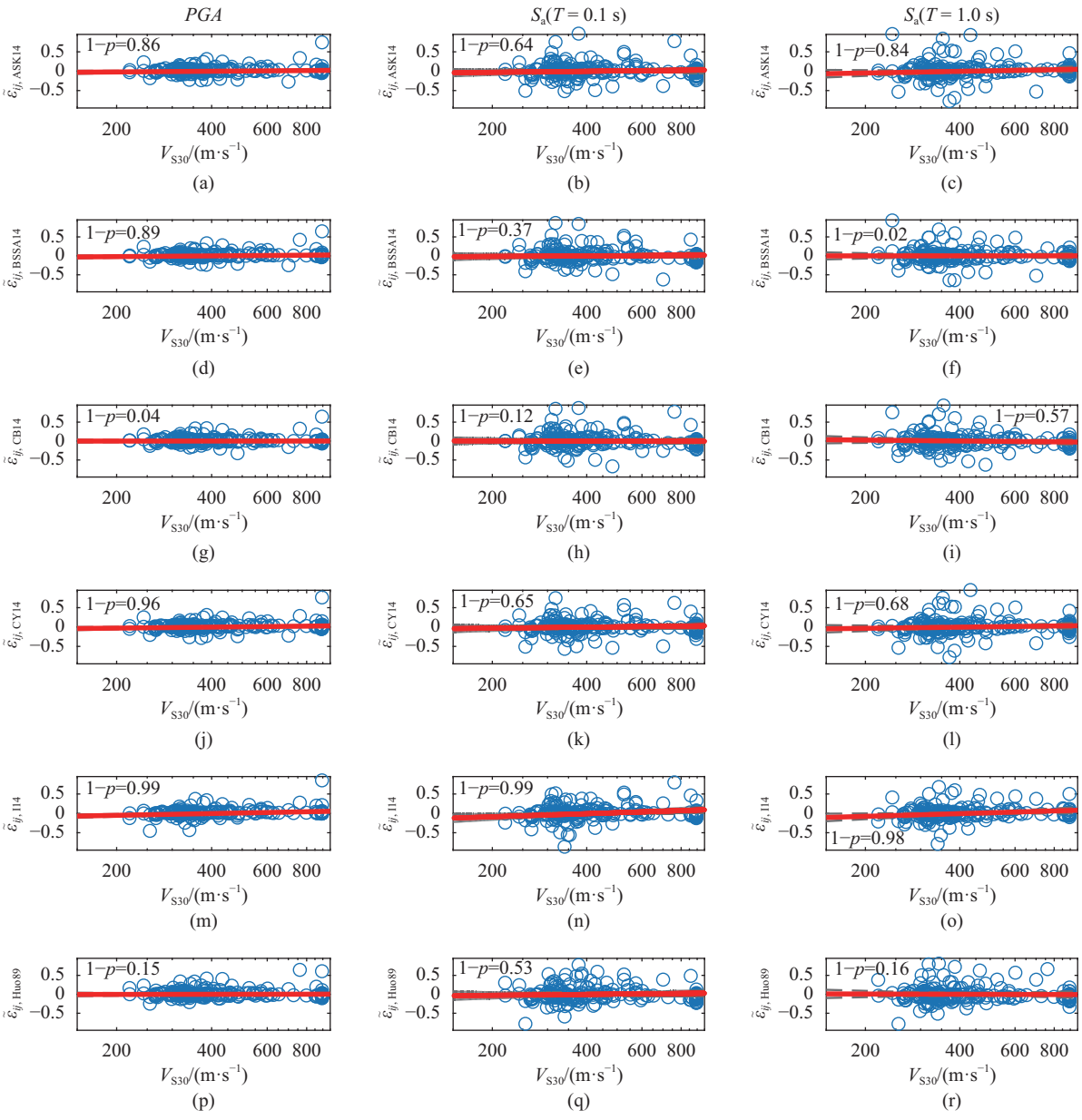

Fig. 6 Variation of updated intra-event residuals against V_{S30} (m/s) for *PGA*, $S_a(T = 0.1$ s), $S_a(T = 1.0$ s)

Shahi et al.[25]. This approach uses wavelet analysis to extract the largest velocity pulse from a given ground motion, which can be used to quantitatively identify those most likely caused by near-fault directivity. Given the records for the three major events in Sichuan, two velocity ground motions $V(t)$ in cm/s at 51DYB and 51MZQ stations in the Wenchuan datasets exhibit impulsive characteristics over a multitude of orientations as pulses indicator (PI) greater than 0.85[26], as shown in Fig. 7. Given the finite-fault model and metadata of the stations, 51DYB station locates in soil-type site with R_{JB} = 49 km and V_{S30} = 374 m/s while 51MZQ station situates in soil-type site with R_{JB} = 5 km and V_{S30} = 766 m/s. The pulse period T_p computed for 51DYB and 51MZQ stations are 6.748 s and 9.366 s, respectively. According to the empirical relationship[26] between T_p and M_W, the expected T_p for Wenchuan earthquake is 9.757 s, which is consistent with the findings in this paper. The 51DYB station is located on the footwall while the 51MZQ sits on the hanging wall of the ruptured fault[15]. The results indicate that there is some evidence of pulse-like ground motions in the Chinese data. However, due to the scarcity of stations of Wenchuan earthquake in the near-field (i.e., 23 stations at a source-to-site distance < 50 km), more detailed investigation regarding the directivity effects, etc. is needed.

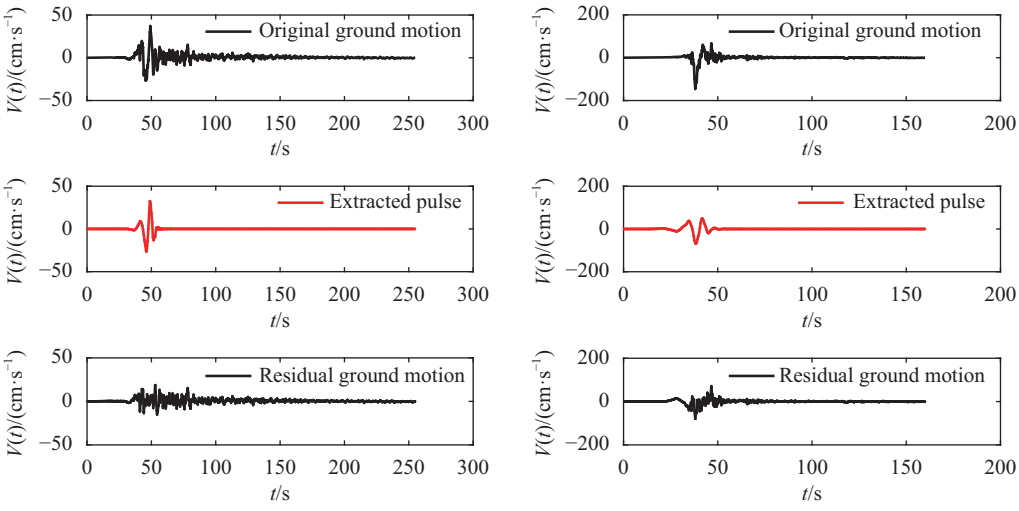

Fig. 7　Pulse-like ground motions observed at the 51DYB and 51MZQ stations in the Wenchuan earthquake

2.6　Code-based spectra and recorded spectra

The current seismic code for building design in China is the Chinese Code for Seismic Design of Buildings (GB50011—2010). It was first released in 1978 and has then been revised in 1989, 2001 and 2010 to implement the latest research and lessons learned during recent domestic and international major earthquake events.

In this Chinese Code for seismic Design of Buildings, the expected performance of a structure is conceptually defined at three levels of seismic hazard: 1) frequent earthquakes, corresponding to a level of the seismic hazard with 63% probability of exceedance in 50 years (i.e., corresponding to a mean return period, T_R, equal to 50 years); 2) moderate earthquakes, corresponding to a level of the seismic hazard with 10% probability of exceedance in 50 years (i.e., T_R equal to 475 years); and 3) rare earthquakes, corresponding to a level of the seismic hazard with 2% probability of exceedance in 50 years (i.e., T_R equal to 2 475 years). Seismic hazard in China is defined in terms of *PGA* and characteristic period of the response spectrum (T_g/s), i.e., the upper limit of the constant spectral acceleration region, refering to the 'moderate' earthquake. These parameters are specified in the Seismic Ground Motion Zoning Maps of China by the CEA. Specifically, the first map is the zoning map in terms of *PGA* with 10% probability of exceedance in 50 years using a seven-level grading system (i.e., < 0.05, 0.05, 0.10, 0.15, 0.20, 0.30*g*, and ≥ 0.40*g*). These *PGA* values are used to determine a seismic intensity to be used for design purposes. The second map consists of three zones (or three seismic group), defined as T_g = 0.35 s, T_g = 0.40 s, and T_g = 0.45 s, respectively, all based on a reference site class Ⅱ. The characteristic period must be adjusted based on the actual site class. The appendix of GB50011—2010 provides a tabulation of seismic intensity, *PGA*, and seismic group for all administrative districts (county or above). The Chinese Code for Seismic Design of Buildings specifies the seismic influence coefficient curve (α), which is comparable to a response spectrum (Fig. 8).

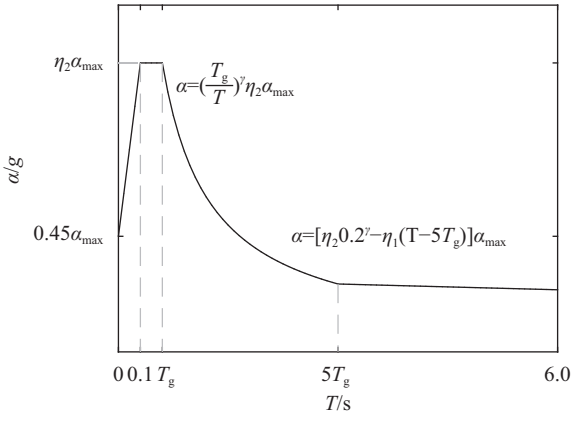

Fig. 8　Design spectrum of spectral accelerations in GB50011—2010

The shape of the response spectrum used to calculate the seismic actions is described by the damping level, the characteristic period T_g in s, and the maximum spectral acceleration α_{max} in g. The critical damping ratio is set as 5% for ordinary structures and it relates to the shape adjustment parameters η_1, η_2 and γ (equation for each of those parameters are provided in the code). The values of α_{max} for the three levels of seismic hazard are

given in the code.

In this section, the code-base spectra for the three mean return periods in GB50011—2010 are visually compared with the median recorded spectra for the three considered events. It is worth pointing out that the median recorded spectra refer to the exponential of the mean of ln (S_a) because it is generally assumed the spectral acceleration S_a follows a log-normal probability distribution. The parameter used to build the code-based spectra are listed in Tab. 3.

Tab. 3 Parameters of spectral acceleration spectra for the three considered events[16–17]

Event	Site class	Seismic intensity	Seismic group	T_g/s	PGA/g	$\alpha_{max,50}/g$	$\alpha_{max,475}/g$	$\alpha_{max,2\,475}/g$
Wenchuan	Ⅱ	Ⅷ	1	0.35	0.20	0.16	0.50	0.90
Lushan	Ⅱ	Ⅶ	2	0.40	0.15	0.12	0.37	0.72
Jiuzhaigou	Ⅱ	Ⅷ	3	0.45	0.20	0.16	0.50	0.90

As shown in Fig. 9, the code-based spectra are consistent in terms of shape with the average recorded spectra and are larger in amplitude than the average recorded spectra across the considered period range and mean return periods of interest.

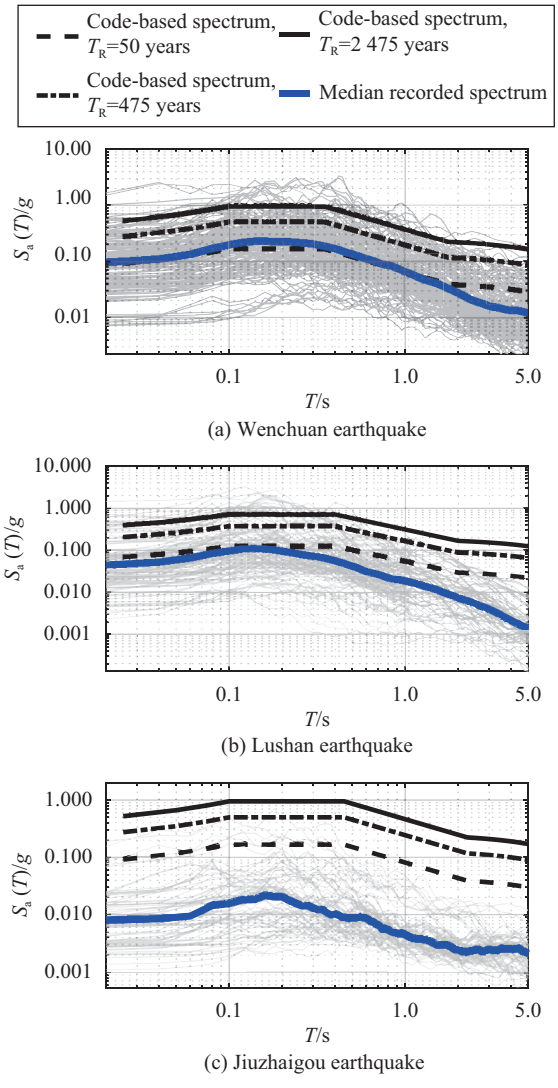

Fig. 9 Code-based spectra and median recorded spectra with 5% damping of the three considered earthquakes

At some stations, the individual recorded spectra (reported in grey in Fig. 9) may exceed the code-based spectra, in particular at short structural periods. The median spectrum of the Wenchuan earthquake in Fig. 9 (a) is slightly higher than the code-based spectrum with T_R = 50 years but smaller than the T_R = 475 years and T_R = 2 475 years spectra.

It is worth noting that the exceedance of code spectra, particularly close to the source of a strong earthquake, does not directly imply inadequacy of PSHA at the basis of the code spectra[27]. This is also because spectra from PSHA, are the results of an 'average' of a series of scenarios considered possible (e.g., small and large source-to-site distances). Such an average may be exceeded close to the source of an earthquake, even if the corresponding scenario is included in the PSHA.

3 Conclusion

This study investigated the compatibility of recent strong motion data in Sichuan Province, China, with state-of-the-art GMPEs established by the NGA-West2 project for shallow crustal earthquakes in active regions and with the local Huo89 model for China. The 2008 M_S 8.0 (M_W 7.9) Wenchuan earthquake, the 2013 M_S 7.0 (M_W 6.6) Lushan earthquake, and the 2017 M_S 7.0 (M_W 6.5) Jiuzhaigou earthquake are considered as case-study events. Using a mixed effects procedure, the analysis first evaluated event terms (inter-event residuals) and intra-event residuals of the Chinese data relative to the NGA-West2 and the Huo89 GMPEs. In particular, source-to-site distance and local site scaling were investigated by examining trends of intra-event residuals with distance and the V_{S30} (i.e., the average shear wave velocity in the upper 30 m) parameter respectively. For the

considered GMPEs, the analysis results show distance dependency in the intra-event residuals of CB14, ASK14, and Huo89 models, particularly at the short period. The V_{S30}-based site dependency is only found in the I14 model. In summary, the NGE-West2 and Huo89 models can be applied for seismic hazard analysis in Sichuan with minor modification of the coefficients regarding the distance scaling and site effect.

A preliminary investigation on near-fault directivity effects and the presence of pulse-like ground motion records in Chinese earthquakes is also carried out. Pulse-like ground motions are observed only at two stations in the Wenchuan earthquake, which may imply some directivity effects. Strong directivity effects in China require more data and further investigation.

Finally, an overview of the design ground motions and the design response spectra in the current Chinese Code for Seismic Design of Buildings is presented. The code-based spectra are compared with the median recorded spectra for the three considered earthquakes. The results show the code spectra are consistent with the observed spectra in terms of amplitude and shape. However, as expected, individual spectra at some sites may exceed the code spectra, in particular at short periods.

While this work has focused on Sichuan Province, the methodology presented here may be applicable elsewhere in China. Future work will formally evaluate data from other regions by using a similar approach to this study.

Acknowledgment

The dataset used in this study is provided by the China Earthquake Data Center owned by the China Earthquake Administration (CEA). The authors would like to thank Prof. MA Qiang, Dr. TAO Dongwang and Mr. LI Jilong from CEA for their support in the data processing. The study presented here is partially funded by the International Center for Collaborative Research on Disaster Risk Reduction (ICCR-DRR), Beijing Normal University, within the China Resilience of Schools to Seismic Hazard (CROSSH) programme. The first author acknowledges the support from China Scholarship Council (CSC).

References:

[1] Huo Junrong.Study on the near-field strong ground motion attenuation law[D].Harbin,China:Institute of Engineering Mechanics,China Earthquake Administration,1989.[霍俊荣.近场强地面运动衰减规律的研究[D].哈尔滨:中国地震局工程力学研究所,1989.]

[2] Hu Yuxianinzheng,Zhang M.A method of predicting ground motion parameters for regions with poor ground motion data[J].Earthquake Engineering and Engineering Vibration,1984,4(1):1–11.[胡聿贤,张敏政.缺乏强震观测资料地区地震动参数的估算方法[J].地震工程与工程震动,1984,4(1):1–11.]

[3] Yu Yanxiang,Li Shanyou,Xiao Liang.Development of ground motion attenuation relations for the new seismic hazard map of China[J].Technology for Earthquake Disaster Prevention,2013,8(1):24–33.[俞言祥,李山有,肖亮.为新区划图编制所建立的地震动衰减关系[J].震灾防御技术,2013,8(1):24–33.]

[4] Abrahamson N A,Silva W J,Kamai R.Summary of the ASK14 ground motion relation for active crustal regions[J].Earthquake Spectra,2014,30(3):1025–1055.

[5] Boore D M,Stewart J P,Seyhan E,et al.NGA-West2 equations for predicting PGA,PGV,and 5% damped PSA for shallow crustal earthquakes[J].Earthquake Spectra,2014,30(3):1057–1085.

[6] Campbell K W,Bozorgnia Y.NGA-West2 ground motion model for the average horizontal components of PGA,PGV,and 5% damped linear acceleration response spectra[J].Earthquake Spectra,2014,30(3):1087–1115.

[7] Chiou B S J,Youngs R R.Update of the Chiou and Youngs NGA model for the average horizontal component of peak ground motion and response spectra[J].Earthquake Spectra,2014,30(3):1117–1153.

[8] Idriss I M.An NGA-West2 empirical model for estimating the horizontal spectral values generated by shallow crustal earthquakes[J].Earthquake Spectra,2014,30(3):1155–1177.

[9] Scasserra G,Stewart J P,Bazzurro P,et al.A comparison of NGA ground-motion prediction equations to Italian data[J].Bulletin of the Seismological Society of America,2009,99(5):2961–2978.

[10] Abrahamson N,Silva W.Summary of the Abrahamson-Silva NGA ground-motion relations[J].Earthquake Spectra,2008,24(1):67–97.

[11] Campbell K W,Bozorgnia Y.NGA ground motion model for the geometric mean horizontal component of PGA,PGV,PGD and 5% damped linear elastic response spectra for periods ranging from 0.01 to 10 s[J].Earthquake Spectra,2008,24(1):139–171.

[12] Chiou B S J,Youngs R R.An NGA model for the average horizontal component of peak ground motion and response spectra[J].Earthquake Spectra,2008,24(1):173–215.

[13] Idriss I M.An NGA empirical model for estimating the horizontal spectral values generated by shallow crustal earthquakes[J].Earthquake Spectra,2008,24(1):217–242.

[14] Boore D M,Atkinson G M.Ground-motion prediction equations for the average horizontal component of PGA,PGV, and 5%-damped psa at spectral periods between 0.01 s and 10.0 s[J].Earthquake Spectra,2008,24(1):99–138.

[15] Wang D,Xie L,Abrahamson N A,et al.Comparison of strong ground motion from the Wenchuan,China,earthquake of 12 May 2008 with the Next Generation Attenuation (NGA) ground-motion models[J].Bulletin of the Seismological Society of America,2010,100(5B):2381–2395.

[16] MOHURD.Code for seismic design of buildings: GB50011—2010[S].Beijing:Ministry of Housing and Urban-Rural Development,2010.[中华人民共和国住房和城乡建设部.建筑抗震设计规范:GB50011—2010[S].北京:中华人民共和国住房和城乡建设部,2010.]

[17] AQSIQ,SAC.Seismic ground motion parameter zonation map of China:GB18306—2015[S].Beijing:AQSIQ, SAC,2015.[中国人民共和国国家质量监督检验检疫总局,中国国家标准化管理委员会.中国地震动参数区划图:GB18306—2015[S].北京:中国人民共和国国家质量监督检验检疫总局,中国国家标准化管理委员会,2015]

[18] Wang Weimin,Zhao Lianfeng,Li Juan,et al.Rupture process of the M_s8.0 Wenchuan earthquake of Sichuan, China[J].Chinese Journal of Geophysics,2008,51(5): 1403–1410.[王卫民,赵连锋,李娟,等.四川汶川8.0级地震震源过程[J].地球物理学报,2008,51(5):1403–1410.]

[19] Wang Weimin,Hao Jinlai,Yao Zhenxing.Preliminary result for rupture process of Apr.20,2013,Lushan earthquake, Sichuan,China[J].Chinese Journal of Geophysics,2013, 56(4):1412–1417.[王卫民,郝金来,姚振兴.2013年4月20日四川芦山地震震源破裂过程反演初步结果[J].地球物理学报,2013,56(4):1412–1417.]

[20] 王卫民,何建坤,郝金来,等.2017年8月8日四川九寨沟7.0级地震震源破裂过程反演初步结果[R/OL].北京:中国科学院青藏高原研究,2017(2017-08-09)[2018-03-01]. http://www.itpcas.ac.cn/xwzx/zhxw/201708/t20170809_4840737.html.

[21] National Earthquake Hazards Reduction Program (US) and Building Seismic Safety Council (US) and United States Federal Emergency Management Agency.NEHRP recommended provisions for seismic regulations for new buildings and other structures:FEMA 450[S].Building Seismic Safety Council,2003.

[22] Yu Yan.Empirical estimate model for ground motion of Wenchuan earthquake zone[D].Harbin:Institute of Engineering Mechanics,China Earthquake Administration, 2012.[喻烟.汶川地震区地震动估计经验模型[D].哈尔滨:中国地震局工程力学研究所,2012.]

[23] USGS.Custom vs30 mapping[DB/OL].(2015-07-26) [2018-03-01].http://earthquake.usgs.gov/hazards/apps/vs30.

[24] Barani S,Albarello D,Spallarossa D,et al.On the influence of horizontal ground-shaking definition on probabilistic seismic-hazard analysis[J].Bulletin of the Seismological Society of America,2015,105(5):2704–2712.

[25] Shahi S K.A probabilistic framework to include the effects of near-fault directivity in seismic hazard assessment[D].Palo Alto:Stanford University,2013.

[26] Baker J W.Quantitative classification of near-fault ground motions using wavelet analysis[J].Bulletin of the Seismological Society of America,2007,97(5):1486–1501.

[27] Iervolino I.Probabilities and fallacies:Why hazard maps cannot be validated by individual earthquakes[J].Earthquake Spectra,2013,29(3):1125–1136.

（编辑 赵 婧）

引用格式: Huang Chen,Galasso Carmine.Engineering analysis of strong motion data from recent earthquakes in Sichuan, China[J].Advanced Engineering Sciences,2018,50(3):112–124.[Huang Chen,Galasso Carmine.Engineering analysis of strong motion data from recent earthquakes in Sichuan, China[J].工程科学与技术,2018,50(3):112–124.]